

## EVLA OBSERVATIONS OF THE RADIO EVOLUTION OF SN 2011dh

M. I. KRAUSS<sup>1</sup>, A. M. SODERBERG<sup>2</sup>, L. CHOMIUK<sup>2,1</sup>, B. A. ZAUDERER<sup>2</sup>, A. BRUNTHALER<sup>3,1</sup>, M. F. BIETENHOLZ<sup>4,5</sup>, R. A. CHEVALIER<sup>6</sup>, C. FRANSSON<sup>7</sup>, M. RUPEN<sup>1</sup>*Draft version December 2, 2024*

## ABSTRACT

We report on Expanded Very Large Array (EVLA) observations of the Type IIb supernova 2011dh, performed over the first 100 days of its evolution and spanning 1–40 GHz in frequency. The radio emission is well-described by the propagation of a self-similar spherical shockwave, generated as the supernova ejecta interact with the local circumstellar environment. Modeling this emission with a standard synchrotron self-absorption (SSA) model gives an average expansion velocity of  $v \approx 0.1c$ , supporting the classification of the progenitor as a compact star ( $R \approx 10^{11}$  cm). We find that the circumstellar density is consistent with a  $\rho \propto r^{-2}$  profile. We determine that the progenitor shed mass at a constant rate of  $4 \times 10^{-5} M_{\odot} \text{ yr}^{-1}$ , assuming a wind velocity of  $1000 \text{ km s}^{-1}$  (values appropriate for a Wolf-Rayet star), or  $9 \times 10^{-7} M_{\odot} \text{ yr}^{-1}$  assuming  $20 \text{ km s}^{-1}$  (appropriate for a yellow supergiant [YSG] star). Both values of the mass-loss rate assume a converted fraction of kinetic to magnetic energy density of  $\epsilon_B = 0.1$ . Although the presence of a YSG is favored by optical imaging, the observed rapid optical evolution and fast expansion argue for a compact progenitor. Furthermore, the excellent agreement of the radio properties of SN 2011dh with the SSA model implies that any YSG companion is likely in a wide, non-interacting orbit, or that interaction with the companion is mitigated by explosion/ejecta asymmetries. Finally, it is possible that the YSG is unrelated and is only coincidentally along the same line of sight.

*Subject headings:* supernovae: individual (SN 2011dh)

## 1. INTRODUCTION

Type IIb supernovae (SNe IIb) were first identified as a distinct class of core-collapse supernova explosions after detailed follow-up observations of the “canonical” Type IIb SN 1993J revealed broad hydrogen and helium features (Filippenko 1997). Recent studies have shown that this spectroscopic class shows a broad diversity in properties including H $\alpha$  strength, profile, and evolution (e.g., compare with SN 2003bg; Matheson et al. 2001; Hamuy et al. 2009; Mazzali et al. 2009). In several cases, yellow supergiant (YSG) stars with extended radii,  $R_* \sim 100 R_{\odot}$ , have been identified at the explosion sites of SNe II (1993J, 2008cn, 2009kr, 2011dh; Maund & Smartt 2009; Maund et al. 2011; Van Dyk et al. 2011; Elias-Rosa et al. 2009, 2010). Yet progenitor diagnostics from multi-wavelength studies indicate that some SNe IIb bear stronger similarity to hydrogen-poor Type Ibc supernovae commonly associated with compact progenitors,  $R_* \approx R_{\odot}$  (hereafter SNe cIIb; Chevalier & Soderberg 2010a). In particular, radio-derived estimates for the shockwave velocity are typically high,  $v \approx 0.1c$ , which is difficult

to explain in the context of shock breakout from an extended object. Along this line of reasoning, stellar evolution tracks place YSGs outside of the SN explosion phase space of the HR diagram (Meynet & Maeder 2005, but see Georgy 2011). Furthermore, some SNe IIb show variable radio light curves indicative of density modulations in the explosion environment, which is likely shaped by the progenitor system (Soderberg et al. 2006; Ryder et al. 2004; Kotak & Vink 2006), and binary companions have been reported for two to date (1993J and 2001ig; Woosley et al. 1994; Ryder et al. 2003; Maund et al. 2007).

Probing the distinguishing differences between SNe cIIb and extended Type IIb supernovae requires early discovery. Since the advent of dedicated transient surveys and improvements in amateur astronomical equipment, such early discoveries are becoming more common. In June 2011, an optical transient was found within the star forming region of M51 by amateur astronomer Amédée Riou (Griga et al. 2011). Prompt spectroscopic follow-up indicated that the object was a supernova of Type II, and further spectroscopy revealed that the object most closely resembled a Type IIb (Arcavi et al. 2011; Marion et al. 2012). A YSG was identified in pre-explosion HST imaging at the position of the SN (Maund et al. 2011; Van Dyk et al. 2011), similar to the case of SN 1993J. However, rapid optical follow-up observations from the Palomar Transient Factory (Law et al. 2009) point to a compact progenitor star as evidenced by its short-lived ( $\Delta t \approx 1$  day) cooling-envelope emission (Arcavi et al. 2011). In our recent paper (Soderberg et al. 2011; hereafter Paper I) we reported the early radio, mm-band and X-ray emission from SN 2011dh. Based on modeling of the

<sup>1</sup> National Radio Astronomy Observatory, Socorro, NM 87801, USA

<sup>2</sup> Harvard-Smithsonian Center for Astrophysics, 60 Garden St., Cambridge, MA 02138, USA

<sup>3</sup> Max-Planck-Institute für extraterrestrische Physik, Giessenbachstraße, 85748 Garching, Germany

<sup>4</sup> Dept. of Physics and Astronomy, York University, Toronto, M3J 1P3, Ontario, Canada

<sup>5</sup> Hartebeesthoek Radio Observatory, P.O. Box 443, Krugersdorp, 1740, South Africa

<sup>6</sup> University of Virginia, Astronomy Department, Charlottesville, VA 22904, USA

<sup>7</sup> Department of Astronomy, The Oskar Klein Centre, Stockholm University, 106 91 Stockholm, Sweden

**Table 1**  
Observed 1–8 GHz Radio Flux Densities (mJy)<sup>a</sup>

Date	MJD	Day <sup>b</sup>	Frequency (GHz)					
			1.4	1.8	2.5	3.5	4.9	6.7
June 17	55729.2	16.4	...	...	...	...	2.430±0.044	4.090±0.063
June 21	55733.2	20.4	< 0.13	< 0.12	0.540±0.079	1.400±0.055	3.150±0.043	4.800±0.055
June 26	55738.2	25.4	0.243±0.079	0.800±0.066	1.626±0.070	2.920±0.061	4.920±0.063	5.980±0.070
July 6	55748.1	35.3	0.331±0.072	1.236±0.067	2.982±0.073	4.908±0.072	6.871±0.091	7.222±0.078
July 16	55758.1	45.3	0.719±0.074	1.858±0.069	4.092±0.083	6.188±0.080	7.836±0.086	6.987±0.077
July 29	55771.0	58.2	2.47±0.12	3.31±0.11	5.84±0.15	7.33±0.14	7.47±0.12	6.11±0.11
Sept 1	55805.7	92.9	3.45±0.11	5.00±0.12	7.02±0.17	6.98±0.13	4.884±0.073	3.941±0.061
enddata								

<sup>a</sup> Quoted upper limits are  $3\sigma$ .

<sup>b</sup> Days from 1 June 2011 (MJD 55712.8).

non-thermal emission, we found that the shockwave velocity was  $v \sim 0.1c$  and thus the explosion bears more similarity to a SN Ibc, typically assumed to be a result of the explosion of a compact Wolf-Rayet star progenitor rather than an extended supergiant. If SN 2011dh did, in fact, have a YSG progenitor, it would be necessary to explain the high shockwave velocity and rapid optical evolution in the context of an extended star.

In this paper, we present spectral energy distribution measurements from our detailed Expanded Very Large Array (EVLA; Perley et al. 2011) observations of SN 2011dh spanning  $\Delta t \approx 100$  days since explosion. This project capitalizes on the nearly continuous band coverage now available from 1–40 GHz with the EVLA. We model the synchrotron emission over 7 epochs to derive the evolution of the shockwave radius and magnetic field as a function of time. We confirm the initial results of Paper I and find that the radio emission over the course of these observations evolves smoothly, with no evidence for the circumstellar density variations seen in other compact SNe Iib.

## 2. OBSERVATIONS AND DATA REDUCTION

We obtained multi-frequency monitoring observations with the EVLA beginning 17 days after explosion (taking  $t_0 = 2011$  May 31.8 UTC) and continuing through day 92 (Program 11A-277: PI Soderberg). These observations comprise seven epochs with a roughly logarithmic cadence, designed to match the expected evolution of the supernova light curves. The second through final epochs covered 1.0–36.5 GHz, utilizing the L (1–2 GHz), S (2–4 GHz), C (4–8 GHz), X (8–8.8 GHz), Ku (12–18 GHz), K (18–26.5 GHz), and Ka-band (26.5–40 GHz) receivers (see Perley et al. 2011 for a description of new observing capabilities with the EVLA). Within each observing band (except X-band),<sup>8</sup> each of two basebands was tuned to a different frequency in order to maximize spectral coverage. We took data with the maximum available 1 GHz of bandwidth per baseband at all bands during the first five epochs, and 128 MHz for the final two. Each epoch was three hours in duration. All observations were performed while the EVLA was in its most extended A-configuration, giving the highest available spatial resolution. EVLA observations were not continued through the subsequent, and most compact, D-configuration, due to concerns about confusion with other sources of radio

<sup>8</sup> Very few wideband X-band receivers were available at the time of our observations. The total bandwidth used at X-band was 0.8 GHz and 256 MHz, respectively.

emission from M51 at lower frequencies (to which the spectral peak of the emission of SN 2011dh had shifted by this time).

Phase reference calibration was carried out using J1335+4542 (1.7° away; 8–40 GHz) or J1327+4326 (3.8° away; 1–8 GHz). At the highest frequencies (> 20 GHz), rapid switching (2 minute cadence) between SN 2011dh and J1335+4542 was done to enable optimal correction for atmospheric phase variations, and referenced pointing was used to correct for antenna pointing offsets. Each observation included data at all bands for the standard flux density calibration source 3C286. Processing was performed with NRAO’s Common Astronomy Software Applications (CASA; McMullin et al. 2007) or Astronomical Image Processing System (AIPS; Greisen 2003), using the same procedure in each.

Bad data identified by the EVLA online system were deleted, as were pure zeros (which may be generated by the correlator as a result of failure); further editing out of radio-frequency interference and poorly performing antennas was done by hand. Frequency-dependent atmospheric opacity was accounted for using the average of a seasonal model and observation-specific information from the weather station (Marvil 2010). At frequencies higher than 5 GHz, where elevation-dependent antenna gain effects become important ( $\gtrsim 1\%$  variance from zenith values), gain curve information was applied at relevant points in the calibration process.

To calibrate the data, a bandpass solution was derived using 3C286; applying this solution, we solved for the complex gains for the calibration sources. We scaled the amplitude gains of the phase calibrator according to the values derived for 3C286 using the “Perley-Butler 2010” flux density standard, and applied these solutions to SN 2011dh.<sup>9</sup> When there was sufficient signal, we performed phase-only self-calibration. We fit a Gaussian model at each frequency to derive integrated flux density values. To estimate the uncertainties on our measured flux densities, we added (in quadrature) errors from the Gaussian fitting with the rms noise of the image, as well as 1% systematic errors at low frequencies (< 20 GHz)

<sup>9</sup> Due to a problem with data acquisition, the flux density calibrator was not present at Ku-band for epoch 3. We characterized the variability of J1335+4542 over the other epochs and found it to be small (RMS of approximately 1% at both 13.5 and 16.0 GHz). We fit its average spectrum and used this model to flux-calibrate the data for SN 2011dh, adding the additional source of error from J1335+4542’s variability in quadrature with the image noise and fit errors to determine the total uncertainty on flux density.

and 3% at high frequencies ( $> 20$  GHz). The integrated flux density values and associated  $1\sigma$  uncertainties are reported in Tables 1 and 2.

### 3. MODELING AND RESULTS

Radio emission from supernovae arises from the interaction of the expanding supernova ejecta with pre-existing circumstellar material, which for a SN IIB is provided by the progenitor’s stellar wind. The interaction of the supernova blast wave with the circumstellar environment takes place in a region that probes recent stellar mass-loss (Chevalier & Fransson 2006). Here, we model the radio emission from SN 2011dh using the standard circumstellar interaction model, described as “model 1” in Chevalier (1996): as the expanding shock moves into the circumstellar medium, the magnetic field strength in the interaction zone increases via turbulence generated in the shocked region. Electrons that have been accelerated to relativistic energies, and whose energy density is assumed to scale as the total postshock energy density, interact with this enhanced magnetic field, producing synchrotron emission. This emission is subject to self-absorption, as further explored by Chevalier (1998); we employ this form of the synchrotron self-absorption (SSA) model to provide an analytic description of the observed radio spectra.

#### 3.1. SSA Model Fits and Derived Parameters

For each given epoch, we fit the radio spectrum using the parameterization

$$S(\nu) = 1.582 S_{\nu_\tau} \left( \frac{\nu}{\nu_\tau} \right)^{5/2} \left\{ 1 - \exp \left[ - \left( \frac{\nu}{\nu_\tau} \right)^{-(p+4)/2} \right] \right\}, \quad (1)$$

where  $S_{\nu_\tau}$  is the flux density at  $\nu_\tau$ , the frequency at which the optical depth is unity, and  $p$  the electron power-law index (Chevalier 1998). We do not see any evidence of external free-free absorption, which would steepen the spectrum for  $\nu < \nu_\tau$  (Chevalier 1998); by contrast, the observed spectra often show excess emission in this regime. Throughout the fitting process, we fixed  $p = 3$ ; allowing  $p$  to vary over the course of the observations yielded values ranging from 2.4–3.4 and did not significantly improve the resulting reduced  $\chi^2$  values. A value of  $p \approx 3$  is typical for observations of SNe Ibc (Chevalier & Fransson 2006), which have similar very similar properties to SNe cIIB. For  $p = 3$ , the observed peak radio flux  $S_{\nu_{\text{op}}}$  occurs at  $\nu_{\text{op}} = 1.14 \nu_\tau$ .

This SSA model provides a good description of the overall observed radio spectra (see Figure 1). However, the formal errors described in §2 are small relative to deviations from the model fits, resulting in large values of  $\chi^2$  and unacceptably small uncertainties on the fitted values of  $S_{\nu_\tau}$  and  $\nu_\tau$ . To correct this, we scaled the fitted uncertainties for each epoch such that the reduced  $\chi^2$  values were unity, equivalent to increasing the errors by a factor of 3–7. These uncertainties were propagated throughout subsequent calculations. We also note that the SSA-derived peak frequencies are systematically  $\approx 10\%$  lower than the apparent peaks, perhaps due to asphericity in the ejecta. Since the trend is consistent over the course of the observations, it will not affect the

time-dependence of the derived parameters. Values for  $S_{\nu_\tau}$  and  $\nu_\tau$ , as well as the parameters derived below, are presented in Table 3.

The fitted spectra can be used as observational tracers of the outer shock radius ( $R_s$ ), strength of the magnetic field ( $B_s$ ), and density of the progenitor’s wind ( $\rho_{\text{wind}}$ ), given a minimal set of assumptions (Chevalier 1998; Chevalier & Fransson 2006):

$$R_s = 4.0 \times 10^{14} \alpha^{-1/19} \left( \frac{f}{0.5} \right)^{-1/19} \left( \frac{D}{\text{Mpc}} \right)^{18/19} \left( \frac{S_{\nu_{\text{op}}}}{\text{mJy}} \right)^{9/19} \times \left( \frac{\nu_{\text{op}}}{5 \text{ GHz}} \right)^{-1} \text{ cm}, \quad (2)$$

$$B_s = 1.1 \alpha^{-4/19} \left( \frac{f}{0.5} \right)^{-4/19} \left( \frac{D}{\text{Mpc}} \right)^{-4/19} \times \left( \frac{S_{\nu_{\text{op}}}}{\text{mJy}} \right)^{-2/19} \left( \frac{\nu_{\text{op}}}{5 \text{ GHz}} \right) \text{ G}, \quad (3)$$

and

$$\rho_{\text{wind}} = A r^{-2} \text{ g cm}^{-3}, \quad (5)$$

where the circumstellar density is parametrized in terms of  $A_* = A/(5 \times 10^{11} \text{ g cm}^{-1})$ , and

$$A_* = 1.0 \alpha^{-8/19} \left( \frac{\epsilon_B}{0.1} \right)^{-1} \left( \frac{f}{0.5} \right)^{-8/19} \left( \frac{D}{\text{Mpc}} \right)^{-8/19} \times \left( \frac{S_{\nu_{\text{op}}}}{\text{mJy}} \right)^{-4/19} \left( \frac{\nu_{\text{op}}}{5 \text{ GHz}} \right)^2 \left( \frac{t}{10 \text{ d}} \right)^2. \quad (6)$$

Here,  $\alpha$  is the ratio of relativistic electron energy density to magnetic energy density ( $\epsilon_e/\epsilon_B$ ),  $f$  is the filling fraction of emitting material,  $D$  is the distance,  $\epsilon_B$  is the converted fraction of kinetic to magnetic energy density, and  $t$  is the age. To calculate values for  $R_s$  and  $B_s$ , we assume equipartition ( $\alpha = 1$ ), and as before,  $p = 3$ . In addition, we take a filling factor of  $f = 0.5$  (as was approximately found for SN 1993J; Bartel et al. 2002), and a distance to M51 of  $8.4 \pm 0.6$  Mpc (Feldmeier et al. 1997; Vinko et al. 2011). The time evolution of the shock radius is consistent with  $R_s \propto t^{0.9}$ , and the magnetic field strength with  $B_s \propto t^{-1}$  (see top and center panels of Figure 2).

The expectation of  $\rho \propto r^{-2}$  may be questionable at large radii, but it is reasonable to approximate the immediate circumstellar environment by assuming a constant progenitor wind (Dwarkadas & Gruszko 2011). These observations probe a region extending to  $\sim 1000$  AU, corresponding to  $\sim 5$  yr for a  $1000 \text{ km s}^{-1}$  wind — much shorter than necessary for substantial wind variability. Given these constraints, and taking  $\epsilon_B = 0.1$ , we find  $A_* \approx 4$ . There is no strong evidence of time variability, suggesting that our assumption of a constant progenitor wind was reasonable (see bottom panel of Figure 2).

We note that in Paper I, joint radio and X-ray model fits pointed to deviations from equipartition,  $\alpha \approx 30$  and  $\epsilon_B \approx 0.01$ , under the assumption that inverse Compton emission dominates the X-ray signal. With these values, our radius estimates are smaller by a factor of 0.8, mag-

**Table 2**  
Observed 8–37 GHz Radio Flux Densities (mJy)<sup>a</sup>

Date	MJD	Day <sup>b</sup>	Frequency (GHz)							
			8.4	13.5	16.0	20.5	25.0	29.0	36.0	
June 17	55729.2	16.4	5.535±0.057	6.970±0.074	6.790±0.073	6.50±0.20	5.13±0.16	4.60±0.14	3.47±0.11	
June 21	55733.2	20.4	5.870±0.060	5.940±0.064	5.313±0.057	4.56±0.14	3.61±0.12	3.117±0.097	2.190±0.074	
June 26	55738.2	25.4	6.935±0.071	5.574±0.080	4.744±0.096	3.70±0.13	2.88±0.11	2.349±0.077	1.644±0.064	
July 6	55748.1	35.3	6.820±0.071	4.334±0.068	3.917±0.073	2.92±0.11	2.53±0.10	2.063±0.073	1.772±0.074	
July 16	55758.1	45.3	6.082±0.064	3.790±0.063	2.960±0.067	2.493±0.097	1.819±0.080	1.549±0.053	1.159±0.051	
July 29	55771.0	58.2	5.097±0.057	2.83±0.14	2.32±0.14	2.35±0.15	1.53±0.16	1.32±0.15	< 0.69	
Sept 1	55805.7	92.9	2.891±0.043	1.627±0.064	1.321±0.072	1.28±0.15	0.71±0.10	0.60±0.11	< 0.42	

<sup>a</sup> Quoted upper limits are  $3\sigma$ .

<sup>b</sup> Days from 1 June 2011 (MJD 55712.8).

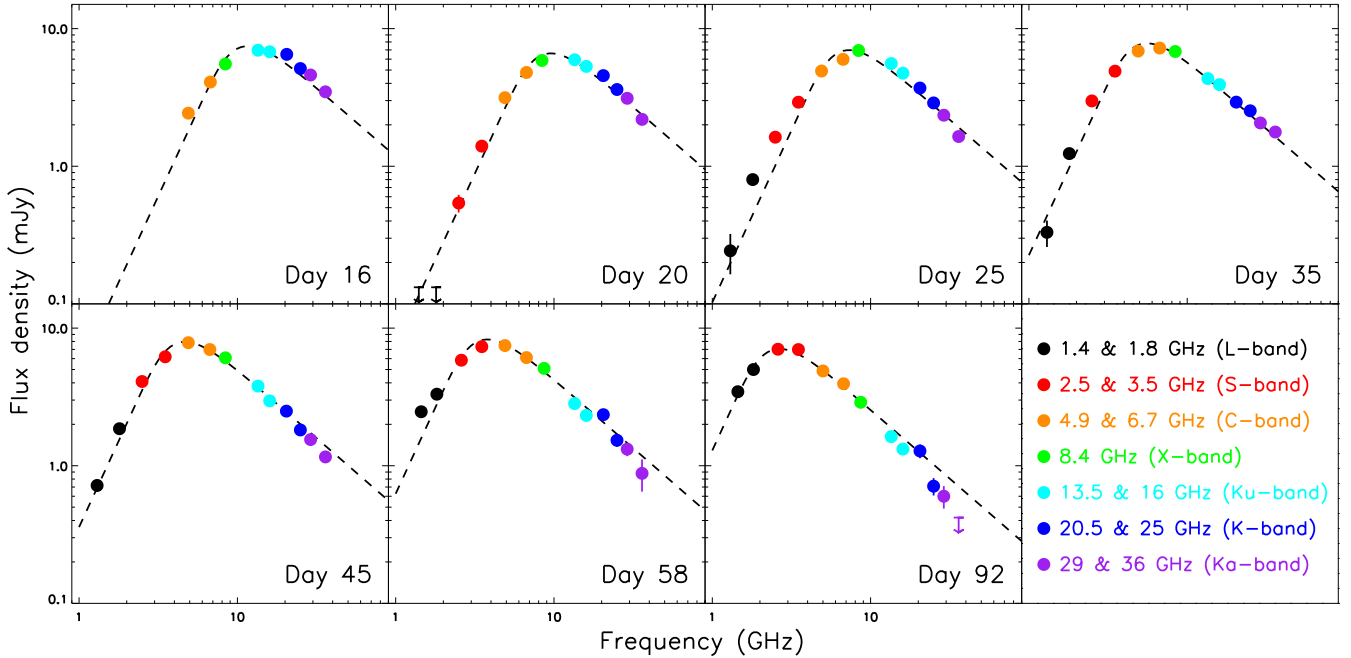


**Figure 1.** EVLA spectra of SN 2011dh. One epoch is shown per panel, labeled by the age of the supernova. Dashed curves show the corresponding SSA model fit. In addition to the errors derived from the Gaussian source fitting and image rms, we include 1% and 3% systematic errors at low ( $< 20$  GHz) and high ( $> 20$  GHz) frequencies, respectively; these are generally smaller than the plotted symbols.

netic field values smaller by a factor of 0.5, and  $A_*$  larger by a factor of 2.

### 3.2. Physical Interpretation

The derived outer shock radii imply a shock velocity of  $dR_s/dt \approx 0.1c$ , confirming the value initially reported in Paper I. Assuming that the supernova ejecta and progenitor wind have power-law density profiles, the evolution of the shock radius with time can be expressed simply as  $R_s \propto t^m$ . For the expected circumstellar density  $\rho_{\text{wind}} \propto r^{-2}$ ,  $m = (n - 3)/(n - 2)$ , where  $n$  is the power-law index of the outer supernova density profile. We find  $m = 0.87 \pm 0.07$ , corresponding to  $n = 9.7^{+12}_{-3.7}$ , which is reasonable for a fast blastwave from a compact progenitor (canonical value of  $m = 0.9$ ; Chevalier 1992). This value of  $m$  is also consistent with joint EVLA-VLBI fits reported in our companion paper (Bietenholz et al. 2012).

The observed decrease in magnetic field strength is also consistent with the standard model for the hydrodynamic

evolution of a self-similar shock. Here, the magnetic energy density ( $\propto B^2$ ) simply scales as the total postshock energy density ( $\propto t^{-2}$ ; Chevalier 1998), thus  $B_s \propto t^{-1}$ . This scaling is a consequence of the fact that the magnetic field generation is thought to arise via turbulence in the shocked region, and is therefore proportional to the total energy density.

We find the scaling factor for the circumstellar density to be consistent with a constant value,  $A_* \approx 4$ , over the course of our observations. This implies a constant mass-loss rate of  $\approx 4 \times 10^{-5} M_\odot \text{ yr}^{-1}$ , assuming a wind velocity of  $1000 \text{ km s}^{-1}$ . These values are in the expected range for a Wolf-Rayet progenitor (Crowther 2007), and agree with what was found in analysis of the early-time radio data (Paper I). Since a change in the assumed velocity results in a linear rescaling of the mass-loss rate ( $\dot{M} = A v_{\text{wind}}$ ), a wind velocity of  $20 \text{ km s}^{-1}$  yields an implied mass-loss rate of  $\approx 9 \times 10^{-7} M_\odot \text{ yr}^{-1}$ , which is reasonable for a YSG progenitor (Georgy 2011).

However, the high shock velocity, as well as the rapid

**Table 3**  
SSA model fits for SN 2011dh

Day <sup>a</sup>	$S_{\nu_\tau}$ (mJy)	$\nu_\tau$ (GHz)	$R_s$ ( $10^{15}$ cm)	$B_s$ (G)	$A_*$ <sup>b</sup>
16.4	$7.26 \pm 0.28$	$10.26 \pm 0.31$	$3.3 \pm 0.4$	$1.33 \pm 0.07$	$3.9 \pm 0.4$
20.4	$6.43 \pm 0.18$	$8.40 \pm 0.20$	$3.8 \pm 0.4$	$1.10 \pm 0.05$	$4.2 \pm 0.3$
25.4	$6.78 \pm 0.24$	$6.43 \pm 0.22$	$5.2 \pm 0.6$	$0.84 \pm 0.04$	$3.7 \pm 0.4$
35.3	$7.60 \pm 0.18$	$4.91 \pm 0.11$	$7.1 \pm 0.7$	$0.63 \pm 0.02$	$4.1 \pm 0.3$
45.3	$7.73 \pm 0.16$	$4.10 \pm 0.09$	$8.6 \pm 0.8$	$0.53 \pm 0.02$	$4.7 \pm 0.4$
58.2	$8.04 \pm 0.23$	$3.34 \pm 0.10$	$11 \pm 1$	$0.43 \pm 0.02$	$5.1 \pm 0.5$
92.9	$6.87 \pm 0.16$	$2.34 \pm 0.05$	$14 \pm 1$	$0.30 \pm 0.01$	$6.6 \pm 0.5$

<sup>a</sup> Days from 1 June 2011 (MJD 55712.8).

<sup>b</sup> In units of  $5 \times 10^{-11}$  g cm<sup>-2</sup>

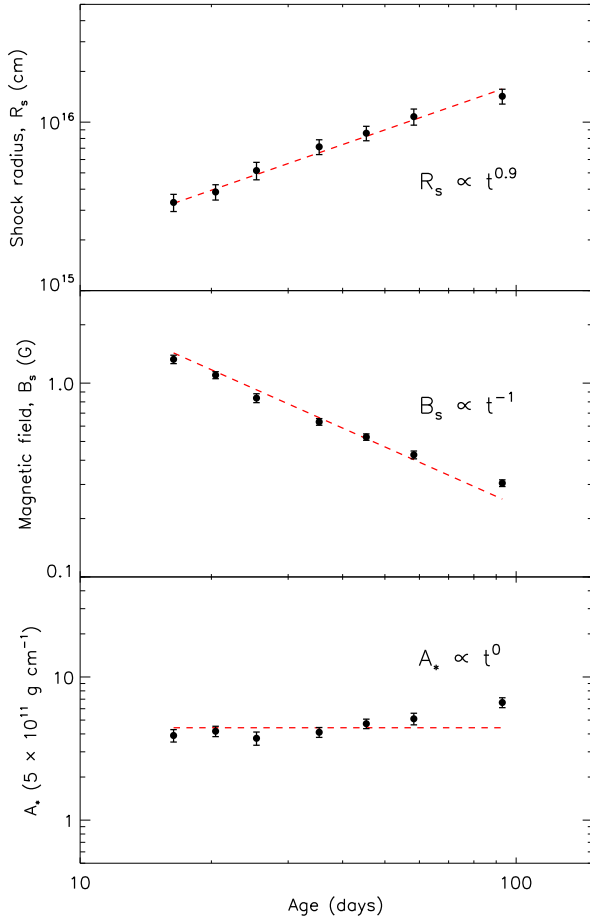


**Figure 2.** Upper panel: shock radius, center panel: magnetic field strength, and lower panel: circumstellar density parameter derived from the per-epoch SSA fits. The expected time behavior for each parameter from the standard model of Chevalier (1996) is shown with dashed lines.

cooling observed in early-time optical spectra, suggest a compact progenitor star for SN 2011dh, and a Type cI Ib classification (Arcavi et al. 2011, Paper I). One observational characteristic of Type cI Ib SNe is that they display late-time radio variability, as seen in SN 2001ig and SN 2003bg (Ryder et al. 2004; Soderberg et al. 2006). We do not yet see evidence of variability in SN 2011dh, but we note that our observations only cover the first  $\sim 100$  days of evolution, which is around the time that variability was discovered in SN 2001ig and SN 2003bg.

#### 4. CONCLUSIONS

The radio spectra of SN 2011dh are well-characterized by an SSA model without any need for additional free-free absorption. This is in contrast with SN 1993J, which required free-free as well as synchrotron self-absorption, and also had a substantially higher derived mass-loss rate ( $A_* \approx 500$ , compared with  $\approx 4$  for SN 2011dh; Fransson & Björnsson 1998). SN 1993J was classified as a SN eI Ib because of its extended progenitor (Chevalier & Soderberg 2010b; Woosley et al. 1994), and the observed differences in absorption and circumstellar density could be characteristic of these two classes of Ib SNe.

However, pre-supernova images of M51 show a YSG co-located with the explosion site, which was suggested as a potential progenitor or binary companion (Maund et al. 2011; Van Dyk et al. 2011; Murphy et al. 2011). Despite this apparent association, the observational agreement with the standard model suggests that there was no appreciable interaction (other than between the supernova ejecta and progenitor wind) within  $\sim 1000$  AU of the explosion site. If the YSG is, in fact, a binary companion, then the orbit must have been quite wide, with an orbital period  $\gtrsim 6000$  yr, and any interaction between this star and the supernova progenitor would have been limited. For comparison, the binary progenitor of SN 1993J likely had an orbital period of  $\sim 2000$  d (Stancliffe & Eldridge 2009), allowing substantial mass transfer to occur and stripping the presupernova star of its H-rich envelope (Woosley et al. 1994). Such an evolutionary scenario would not be possible for SN 2011dh, even if the YSG was associated with the system. Alternatively, if the blast wave were highly asymmetric, interaction with a more nearby companion could have been avoided; we consider this unlikely, since the radio data agree quite well with the standard, spherical ejecta model. Moreover, the lifetime of the YSG phase is estimated at just 3000 yr (Drout et al. 2009), making it improbable that the YSG would happen to be in this phase at the time of its companion's explosion.

Another possibility is that the YSG is itself the supernova progenitor, but this would require a process to enable the escape of fast shockwaves from YSGs, either through steep ejecta density profiles or ejecta asymmetries (jets). Future observations, including optical imaging of the field after SN 2011dh has faded, will help determine any association with the YSG and the true nature of the progenitor system.

The National Radio Astronomy Observatory is a facility of the National Science Foundation operated under cooperative agreement by Associated Universities, Inc. A. B. was supported by a Marie Curie Outgoing International Fellowship (FP7) of the European Union (project number 275596). We acknowledge with thanks the variable star observations from the AAVSO International database contributed by observers worldwide and used in this research. This research has made use of NASA's Astrophysics Data System Bibliographic Services.

## REFERENCES

- Arcavi, I., Gal-Yam, A., Yaron, O., et al. 2011, *ApJ*, 742, L18
- Bartel, N., Bietenholz, M. F., Rupen, M. P., et al. 2002, *ApJ*, 581, 404
- Bietenholz, M. F., Brunthaler, A., Bartel, N., et al. 2012, submitted
- Chevalier, R. A. 1992, *ApJ*, 394, 599
- Chevalier, R. A. 1996, in *Astronomical Society of the Pacific Conference Series*, Vol. 93, *Radio Emission from the Stars and the Sun*, ed. A. R. Taylor & J. M. Paredes, 125
- . 1998, *ApJ*, 499, 810
- Chevalier, R. A., & Fransson, C. 2006, *ApJ*, 651, 381
- Chevalier, R. A., & Soderberg, A. M. 2010a, *ApJ*, 711, L40
- . 2010b, *ApJ*, 711, L40
- Crowther, P. A. 2007, *ARA&A*, 45, 177
- Drout, M. R., Massey, P., Meynet, G., Tokarz, S., & Caldwell, N. 2009, *ApJ*, 703, 441
- Dwarkadas, V. V., & Gruszko, J. 2011, *ArXiv e-prints*
- Elias-Rosa, N., Van Dyk, S. D., Li, W., et al. 2009, *ApJ*, 706, 1174
- . 2010, *ApJ*, 714, L254
- Feldmeier, J. J., Ciardullo, R., & Jacoby, G. H. 1997, *ApJ*, 479, 231
- Filippenko, A. V. 1997, *ARA&A*, 35, 309
- Fransson, C., & Björnsson, C.-I. 1998, *ApJ*, 509, 861
- Georgy, C. 2011, *ArXiv e-prints*
- Greisen, E. W. 2003, *Information Handling in Astronomy - Historical Vistas*, 285, 109
- Griga, T., Marulla, A., Grenier, A., et al. 2011, *Central Bureau Electronic Telegrams*, 2736, 1
- Hamuy, M., Deng, J., Mazzali, P. A., et al. 2009, *ApJ*, 703, 1612
- Kotak, R., & Vink, J. S. 2006, *A&A*, 460, L5
- Law, N. M., Kulkarni, S. R., Dekany, R. G., et al. 2009, *PASP*, 121, 1395
- Marion et al. 2012, in preparation
- Marvil, J. 2010, *EVLA Memo 143: Improving the frequency resolution of the default atmospheric opacity model*
- Matheson, T., Filippenko, A. V., Li, W., Leonard, D. C., & Shields, J. C. 2001, *AJ*, 121, 1648
- Maund, J. R., & Smartt, S. J. 2009, *Science*, 324, 486
- Maund, J. R., Wheeler, J. C., Patat, F., et al. 2007, *ApJ*, 671, 1944
- Maund, J. R., Fraser, M., Ergon, M., et al. 2011, *ApJ*, 739, L37
- Mazzali, P. A., Deng, J., Hamuy, M., & Nomoto, K. 2009, *ApJ*, 703, 1624
- McMullin, J. P., Waters, B., Schiebel, D., Young, W., & Golap, K. 2007, in *Astronomical Society of the Pacific Conference Series*, Vol. 376, *Astronomical Data Analysis Software and Systems XVI*, ed. R. A. Shaw, F. Hill, & D. J. Bell, 127
- Meynet, G., & Maeder, A. 2005, *A&A*, 429, 581
- Murphy, J. W., Jennings, Z. G., Williams, B., Dalcanton, J. J., & Dolphin, A. E. 2011, *ApJ*, 742, L4
- Perley, R. A., Chandler, C. J., Butler, B. J., & Wrobel, J. M. 2011, *ApJ*, 739, L1
- Ryder, S. D., Sadler, E., Subrahmanyan, R., et al. 2003, *ArXiv Astrophysics e-prints*
- Ryder, S. D., Sadler, E. M., Subrahmanyan, R., et al. 2004, *MNRAS*, 349, 1093
- Soderberg, A. M., Chevalier, R. A., Kulkarni, S. R., & Frail, D. A. 2006, *ApJ*, 651, 1005
- Soderberg, A. M., Margutti, R., Zauderer, B. A., et al. 2011, *ArXiv e-prints*
- Stancliffe, R. J., & Eldridge, J. J. 2009, *MNRAS*, 396, 1699
- Van Dyk, S. D., Li, W., Cenko, S. B., et al. 2011, *ApJ*, 741, L28
- Vinko, J., Takats, K., Szalai, T., et al. 2011, *ArXiv e-prints*
- Woosley, S. E., Eastman, R. G., Weaver, T. A., & Pinto, P. A. 1994, *ApJ*, 429, 300